Quaternary International 682 (2024) 46–59

Contents lists available at ScienceDirect

Quaternary International

journal homepage: www.elsevier.com/locate/quaint

Revisiting the physical processes controlling the tropical atmospheric circulation changes during the Mid-Piacenzian Warm Period

Ke Zhang [a], Yong Sun [b,*], Zhongshi Zhang [c,d], Christian Stepanek [e], Ran Feng [f], Daniel Hill [g], Gerrit Lohmann [e,h], Aisling Dolan [g], Alan Haywood [g], Ayako Abe-Ouchi [i], Bette Otto-Bliesner [j], Camille Contoux [k], Deepak Chandan [l], Gilles Ramstein [k], Harry Dowsett [m], Julia Tindall [g], Michiel Baatsen [n], Ning Tan [o], William Richard Peltier [l], Qiang Li [p], Wing-Le Chan [i], Xin Wang [a], Xu Zhang [a,b,**]

[a] *Key Laboratory of Western China's Environmental Systems (Ministry of Education), College of Earth and Environmental Sciences, Lanzhou University, Lanzhou, Gansu, 730000, China*
[b] *State Key Laboratory of Tibetan Plateau Earth System, Resources and Environment (TPESRE), Institute of Tibetan Plateau Research, Chinese Academy of Sciences, Beijing, 100101, China*
[c] *Department of Atmospheric Science, School of Environmental Studies, China University of Geosciences, Wuhan, Hubei, 430074, China*
[d] *NORCE Norwegian Research Centre, Bjerknes Centre for Climate Research, Bergen, Norway*
[e] *Alfred Wegener Institute – Helmholtz Centre for Polar and Marine Research, Bremerhaven, Germany*
[f] *Department of Geosciences, University of Connecticut, Storrs, USA*
[g] *School of Earth and Environment, University of Leeds, Woodhouse Lane, Leeds, LS2 9JT, UK*
[h] *Institute for Environmental Physics, University of Bremen, Bremen, Germany*
[i] *Atmosphere and Ocean Research Institute, University of Tokyo, Kashiwa, Japan*
[j] *Climate and Global Dynamics Laboratory, National Center for Atmospheric Research, (NCAR), Boulder, CO, 80305, USA*
[k] *Laboratoire des Sciences Du Climat et de l'Environnement, LSCE/IPSL, CEA-CNRS-UVSQ, Université Paris-Saclay, Gif-sur-Yvette, France*
[l] *Department of Physics, University of Toronto, Toronto, M5S 1A7, Canada*
[m] *U.S. Geological Survey, Florence Bascom Geoscience Center, MS 926A, 12201 Sunrise Valley Drive, Reston, VA, 20192, USA*
[n] *Centre for Complex Systems Science, Utrecht University, Utrecht, the Netherlands*
[o] *Key Laboratory of Cenozoic Geology and Environment, Institute of Geology and Geophysics, Chinese Academy of Sciences, Beijing, 100029, China*
[p] *Department of Physical Geography and Bolin Centre for Climate Research, Stockholm University, Stockholm, Sweden*

ARTICLE INFO

Keywords:
Pliocene
PlioMIP2
Hadley circulation
Walker circulation
Diabatic heating/cooling
Subtropical baroclinicity

ABSTRACT

The Mid-Piacenzian Warm Period (MPWP; 3.0–3.3 Ma), a warm geological period about three million years ago, has been deemed as a good past analog for understanding the current and future climate change. Based on 12 climate model outputs from Pliocene Model Intercomparison Project Phase 2 (PlioMIP2), we investigate tropical atmospheric circulation (TAC) changes under the warm MPWP and associated underlying mechanisms by diagnosing both atmospheric static stability and diabatic processes. Our findings underscore the advantage of analyzing atmospheric diabatic processes in elucidating seasonal variations of TAC compared to static stability assessments. Specifically, by diagnosing alterations in diabatic processes, we achieve a quantitative understanding and explanation the following TAC changes (incl. Strength and edge) during the MPWP: the weakened (annual, DJF, JJA) Northern Hemisphere and (DJF) Southern Hemisphere Hadley circulation (HC), reduced (annual, DJF) Pacific Walker circulation (PWC) and enhanced (annual, JJA) Southern Hemisphere HC and (JJA) PWC, and westward shifted (annual, DJF, JJA) PWC. We further addressed that the increasing bulk subtropical static stability and/or decreasing vertical shear of subtropical zonal wind - two crucial control factors for changes in subtropical baroclinicity - may promote HC widening, and vice versa. Consequently, our study of spatial diabatic heating and cooling, corresponding to upward and downward motions within the TAC, respectively,

---

* Corresponding author.

** Corresponding author. Key Laboratory of Western China's Environmental Systems (Ministry of Education), College of Earth and Environmental Sciences, Lanzhou University, Lanzhou, Gansu, 730000, China.

E-mail addresses: yongsun@itpcas.ac.cn (Y. Sun), xu.zhang@itpcas.ac.cn (X. Zhang).

https://doi.org/10.1016/j.quaint.2024.01.001
Received 14 December 2023; Received in revised form 31 December 2023; Accepted 2 January 2024

provides a new perspective for understanding the processes controlling seasonal TAC changes in response to surface warming.

1. Introduction

The Mid-Piacenzian Warm Period (MPWP, ~3.264~3.025 Ma) was a geologically warm period about 3 million years ago (McClymont et al., 2020; Dowsett et al., 2016; Haywood et al., 2013). This period was similar to the present-day in many aspects, such as land-sea distribution and CO_2 concentrations (~400 ppm) (Zhang et al., 2022; Haywood et al., 2016; Martínez-Botí et al., 2015; Bartoli et al., 2011; Pagani et al., 2010). Therefore, the MPWP climate is often used for comparison to today's climate. The MPWP climate has also been considered as a future analogue of today's climate, because it has higher global surface temperatures compared to the pre-industrial (PI) period (1.7–5.2 °C) (Berntell et al., 2021; McClymont et al., 2020; Tierney et al., 2020; Haywood et al., 2020, 2013; Burke et al., 2018; Dowsett et al., 2016, 2013; IPCC Jansen et al., 2007).

Climate reconstructions and proxy data syntheses, as well as model simulations have been conducted to examine the large-scale features of the MPWP (Feng et al., 2022; Haywood et al., 2013, 2020, 2013; Dowsett et al., 2013, 2016; Pound et al., 2014; Salzmann et al., 2013). The Pliocene Research, Interpretation and Synoptic Mapping (PRISM) is an ongoing project, begun over 30 years ago, to extract the MPWP climate signal from proxy data and to provide the boundary conditions for conducting climate simulations during the Pliocene (Haywood et al., 2000, 2013, 2020; Sun et al., 2018; Dowsett et al., 2016; Sun et al., 2016; Dowsett et al., 2011; Sloan et al., 1996; Chandler et al., 1994; Dowsett et al., 1994, 1999). Global surface warming during the MPWP compared to the PI is 1.8–3.6 °C in PlioMIP1 and 1.7–5.2 °C in PlioMIP2, respectively (Baatsen et al., 2021; Zhang et al., 2021; Chan and Abe-Ouchi, 2020; Feng et al., 2020; Haywood et al., 2020, 2013; Li et al., 2020; Tan et al., 2020; Hunter et al., 2019; Zheng et al., 2019; Chandan and Peltier, 2018). The MPWP surface warming is spatially heterogeneous, with more pronounced warming in the polar regions than in the lower latitudes (e.g., Haywood et al., 2020, 2013; Hopcroft et al., 2020), and land warming is higher than ocean (Haywood et al., 2020). Within PlioMIP2, the MPWP surface warming is found to be caused by increased CO_2 concentrations, paleogeographic changes (Chan and Abe-Ouchi, 2020; Haywood et al., 2020; Stepanek et al., 2020; Chandan and Peltier, 2018; Kamae et al., 2016), prescribed vegetation and ice sheet state (Feng et al., 2022; Haywood et al., 2020; Lunt et al., 2010).

Tropical atmospheric circulation which consists mainly of the meridional overturning circulation (Hadley circulation, HC) and the zonal overturning circulation (Walker circulation, WC), plays an important role in maintaining the precipitation pattern in low and middle latitudes. Considerable efforts have been made to investigate the changes in the intensity and boundary of the tropical atmospheric circulation in the current climate context, as well as the future projections of the weakening of the strength and shifting of the boundary of the atmospheric circulation (Xia et al., 2020; Hu et al., 2013; Sun et al., 2013). Tropical atmospheric circulation has undergone significant changes during the MPWP. For example, the HC was weakened in strength and the boundary expanded towards the poles (Feng et al., 2020; Corvec and Fletcher, 2017). The ascending branch of WC in the Indo-Pacific warm pool (IPWP) moved westward (Han et al., 2021; Hunter et al., 2019; Kamae et al., 2011, 2016; Sun et al., 2013). Many studies have extensively investigated the mechanisms behind changes in tropical atmospheric circulation, such as Adam et al. (2014) showed that the HC poleward shift during the observational period and modeling studies suggested that the HC poleward shift and weakening strength during the Pliocene all caused by global warming and the weakened meridional temperature gradient (Sun et al., 2013; Brierley et al., 2009). Kamae et al. (2011) used the model MRI-CGCM2.3 to study HC and WC changes, and concluded that weakened intensities of both were caused by reduced meridional and zonal temperature gradients, respectively. Subsequent analyses suggested that changes in topography and vegetation during the MPWP were the dominant contributors to HC changes, but a detailed mechanism was not presented (Kamae et al., 2016). Using the model IPSL-CM5A-LR, Sun et al. (2013) analyzed the changes and mechanisms of HC and WC, but lacked a comparison with other PlioMIP models. Feng et al. (2020) analyzed the strengths of HC and WC during the MPWP period using three versions of the CESM model and stated that both HC and WC were weakened, and explained the weakened HC by the change of meridional temperature gradient and the weakened WC via a link to the El Niño phenomenon. Using multiple PlioMIP2 models to analyze the boundary change of HC and WC, it is shown that HC is influenced by the movement of ITCZ to the north, and WC continues to move to the west. However, detailed mechanistic explanation is not given (Han et al., 2021).

In addition, changes in the static stability of the tropical and subtropical atmosphere are another frequently used indicator to explain the weakening strength and boundary shifts in the tropical atmospheric circulation in different climate backgrounds. The weakened HC and WC are often qualitatively interpreted by increased static stability of the upper tropical atmosphere, but this interpretation is also controversial (Chemke and Polvani, 2021; Seo et al., 2014; Mitas and Clement, 2006), especially since the seasonal enhancement of HC and WC still corresponds to increased static stability. The increased static stability of the atmospheric in the subtropics prevents the penetration of baroclinicity Rossby wave from mid-latitudes into the subtropics, which in turn explains the poleward shift of the HC boundary (Lu et al., 2007). However, the contribution of vertical zonal wind shear - another important factors affecting the baroclinicity of the subtropic - to the shift in the HC boundary during the MPWP is not well understood. In short, previous studies of tropical atmospheric circulation during MPWP have either been based on single-model analyses or have not explored underlying mechanisms in detail (Corvec and Fletcher, 2017; Kamae et al., 2011).

In this study, we (1) use PlioMIP2 models to perform a comprehensive and systematic analysis of the characteristics and physical processes of HC and WC changes in the Pliocene; (2) provide a new perspective to quantitatively explain changes in the intensity of annual and seasonal HC and WC, and as well as WC position shifts, via tropical diabatic processes; (3) clarify the relative contribution of two factors (static stability and vertical wind shear) affecting the baroclinicity of the subtropical atmosphere to the shifts of the HC boundary during the MPWP.

2. Data and methods

2.1. PlioMIP2 models

We analyzed the changes in the tropical atmospheric circulation during the MPWP based on the Pliocene Model Intercomparison Project Phase 2 (PlioMIP2) model ensemble (see Table 1 for details). Exposing the various models to the same boundary conditions from PRISM4 when performing MPWP simulations (Eoi400) enables direct comparisons among different model's outputs. In particular, the PRISM4 MPWP boundary conditions comprise closure of the Bering Strait, the Canadian Arctic Islands being part of a land connection, a reduction of the Greenland Ice Sheet area to 25% of its current size, and the CO_2 level being set to 400 ppmv (Haywood et al., 2021; Dowsett et al., 2016; Haywood et al., 2016). In addition to simulation Eoi400, each participating model needed to carry out a PI control experiment (E280), and the CO_2 level being set to 280 ppmv. We select the last 30 years of modeling outputs to represent the corresponding climatology in each model for the last 30 years have reached a state of equilibrium.

2.2. Analysis methods

2.2.1. Diagnosis method of tropical circulation

The mass stream function (MSF) is the most widely used method to describe the zonal mean meridional circulation as the derivation of MSF follows the conservation of mass (Zhang et al., 2023; Sun et al., 2019; Nguyen et al., 2018; Hu et al., 2018; Feng et al., 2016, 2015; Oort and Yienger, 1996). A brief description for the deduction of the MSF is given as follows: if the circulation has no mass flux (i.e., no mass divergence) in zonal direction, it can be expressed as $\frac{\partial v}{\partial y}+\frac{\partial \omega}{\partial p}=0$, where v is the meridional velocity along the latitude axis y, and ω is the vertical velocity along the pressure axis p (Hu et al., 2018). According to the mathematical law, there must exist an MSF that can describe both the meridional and vertical motions (Cook, 2003):

Table 1
Details of the PlioMIP2 models used in this study.

Model ID	Sponsor(s), Country	Atmosphere Top Resolution & Model References	Ocean Resolution Z Coord., Top BC, & Model References	Vegetation (Static – Salzmann et al., 2008 or Dynamic)	References
CESM 1.0.5	IMAU, Utrecht University, the Netherlands	CAM4 Top = 2 hPa FV (2.5° × 1.9°) L26 Neale et al. (2010)	POP2 Bipolar Curvilinear 320° × 384°(formal 1°) L60 Smith et al. (2010)	Salzmann et al. (2013)	Baatsen et al. (2021)
CCSM4-UofT	University of Toronto, Canada	Top = 2Pa FV1.25° × 0.9° L26 Neale et al. (2010)	0.27 °–0.54° × 1.1° L60, Depth, free surface Smith et al. (2010), Danabasoglu et al. (2012), Chandan and Peltier (2018)	Salzmann et al. (2013)	Chandan and Peltier (2018) Peltier and Vettoretti (2014)
CESM2	National Center for Atmospheric Research	Top = 2 hPa FV0.9° × 1.25° (~1°) L32 (CAM6) (Danabasoglu et al., 2020)	G16 (~1°), L60 depth, rigid lid, updated mixing scheme	Salzmann et al. (2013)	Feng et al. (2020)
COSMOS	Alfred Wegener Institute, Germany	Top = 10 hPa T31 (3.75° × 3.75°), L19 Roeckner et al. (2003)	Bipolar orthogonal curvilinear GR30, L40 depth, free surface Marsland et al. (2003)	Dynamic	Stepanek et al. (2020)
EC-Earth 3.3	Stockholm University, Sweden	IFS cycle 36r4 Top = 5 hPa 1.125° × 1.125° L62 Döscher et al. (2020)	NEMO3.6, ORAC1 1.0° × 1.0°, L46 Madec (2008)	Salzmann et al. (2013)	Zheng et al. (2019)
GISS-E2-1-G	Goddard Institute for Space Studies, United States of America	Top = 0.1 mb 2.0° × 2.5°, L40 Kelley et al. (2020)	1.0° × 1.25°, P*, free surface Kelley et al. (2020)	Salzmann et al. (2013)	Chandler et al. (2013)
HadCM3	University of Leeds, United Kingdom	Top = 5 hPa 2.5° × 3.75°, L19 Pope et al. (2000)	1.25° × 1.25°, L20 Depth, rigid lid Gordon et al. (2000)	Salzmann et al. (2013)	Hunter et al. (2019)
IPSL-CM6A-LR	Laboratoire des Sciences du Climat et de l'Environnement (LSCE), France	Top = 1 hPa 2.5° × 1.26°, L79 Hourdin et al. (2020)	1° × 1°, refined at 1/3° in the tropics, L75 Free surface, Z- coordinates Madec et al. (2017)	Salzmann et al. (2013)	Lurton et al. (2020)
IPSLCM5A2.1	LSCE France	Top = 70 km 3.75° × 1.9°, L39 Hourdin et al. (2006, 2013) Sepulchre et al. (2020)	0.5°–2° × 2°, L31 Free surface, Z- coordinates Dufresne et al. (2013); Madec and Imbard (1996); Sepulchre et al. (2020)	Salzmann et al. (2013)	Tan et al. (2020)
IPSLCM5A	LSCE France	Top = 70 km 3.75° × 1.9°, L39 Hourdin et al. (2006, 2013)	0.5°–2° × 2°, L31 Free surface, Z- coordinates Dufresne et al. (2013); Madec and Imbard (1996)	Salzmann et al. (2013)	Contoux et al. (2012)
MIROC4m	Center for Climate System Research (Uni. Tokyo), National Inst. For Env. Studies, Frontier Research Center for Global Change, (JAMSTEC), Japan	Top = 30 km T42 (~2.8° × 2.8°) L20 K-1 Developers (2004)	0.5 °–1.4° × 1.4°, L43 Sigma/depth free surface K-1 Developers (2004)	Salzmann et al. (2013)	Chan and Abe-Ouchi (2020)
NorESM-F	NORCE Norwegian Research Centre, Bjerknes Centre for Climate Research, Bergen, Norway	Top = 3.5 hPa 1.9° × 2.5°, L26 (CAM4)	~1° × 1°, L53 isopycnal layers	Salzmann et al. (2013)	Li et al. (2020)

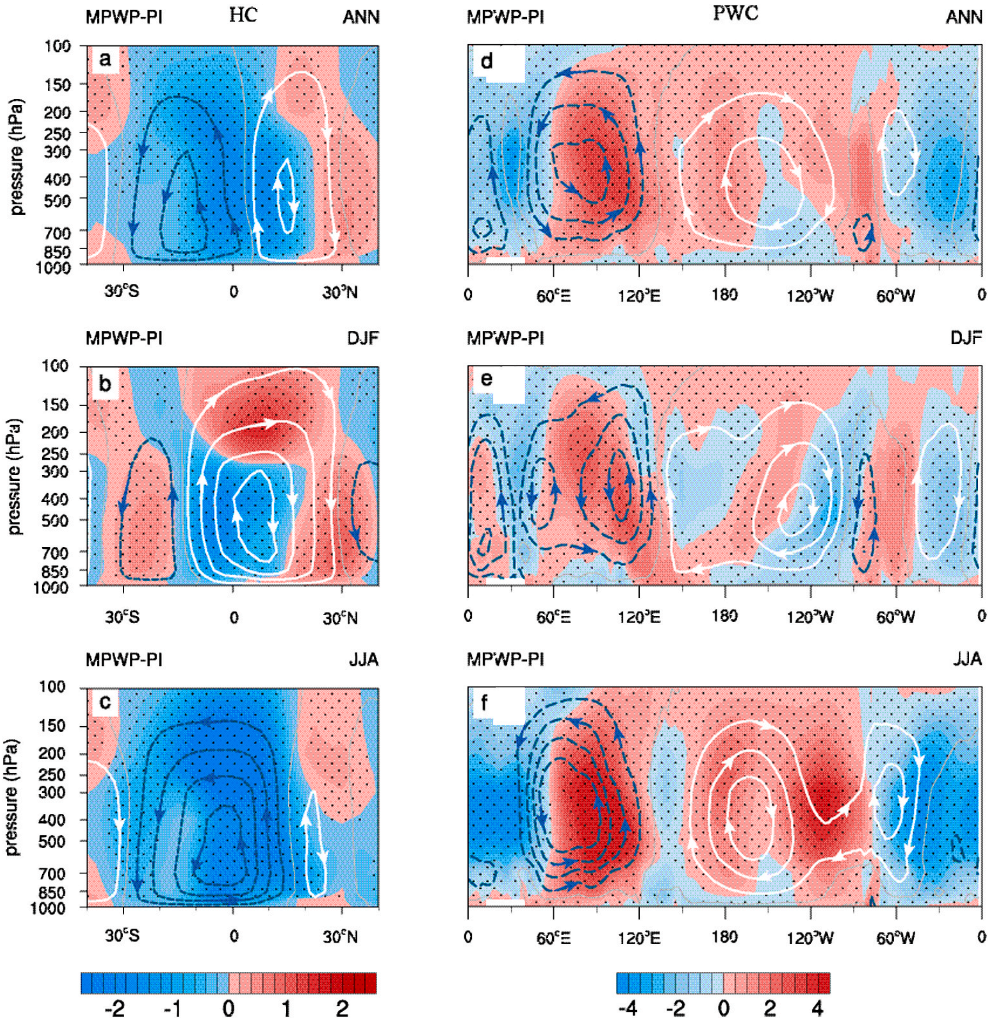

Fig. 1. The changes of mass stream function (left) and Walker circulation stream function (right) in Mid-Piacenzian warm period (MPWP; units: 10^{10} kg/s; shaded) relative to pre-industrial (PI; units: 10^{10} kg/s; contours) in terms of annual mean (top panel), boreal winter (December-January-February, DJF, middle panel) and boreal summer (June-July-August, JJA, bottom panel), as inferred from the Pliocene Model Intercomparison Project Phase 2 (PlioMIP2) multi-model ensemble (MME) average. The arrows in the figure diagram illustrate the direction of the atmospheric circulation, white indicates clockwise circulation, blue indicates counterclockwise circulation.

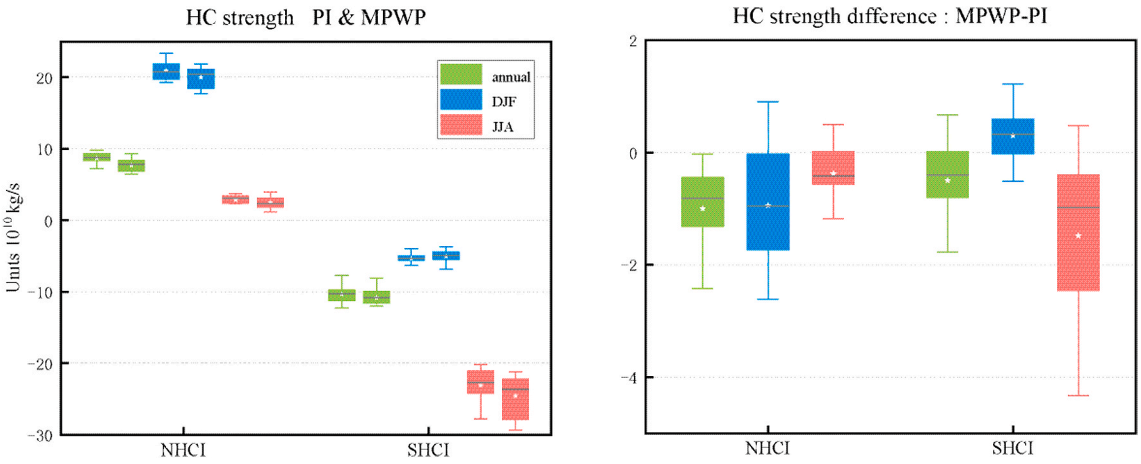

Fig. 2. Boxplots show the strengths of HC in two periods: PI and MPWP (left panel) and differences between MPWP and PI period (right panel). NHCI (SHCI) is the intensity of HC in the Northern (Southern) Hemisphere, respectively. The green, blue and red colors are used to distinguish the results of annual mean, DJF, JJA, respectively.

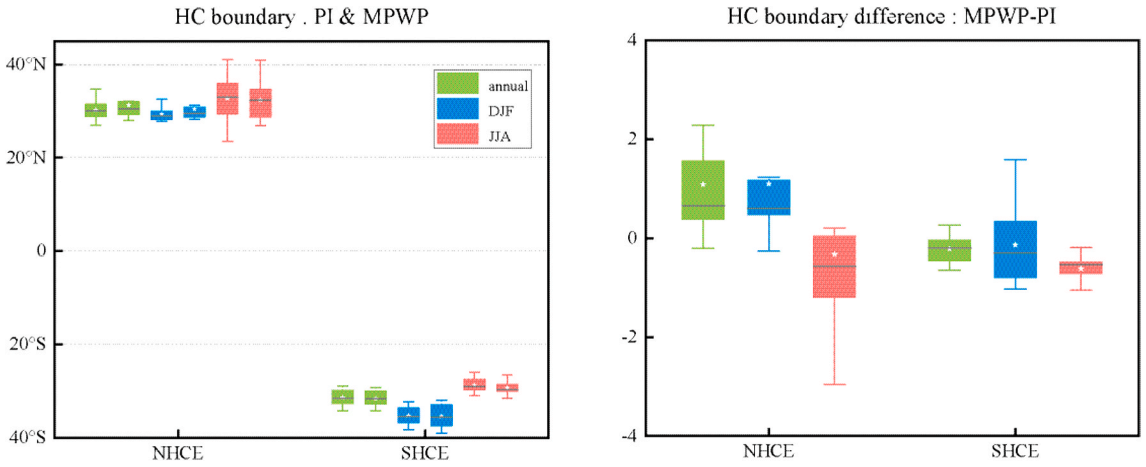

Fig. 3. Same as Fig. 2, except that boxplots show the Northern and Southern boundaries of HC in two periods: PI and MPWP (left panel) and differences between MPWP and PI period (right panel). NHCE (SHCE) is the edge of HC in the Northern (Southern) Hemisphere.

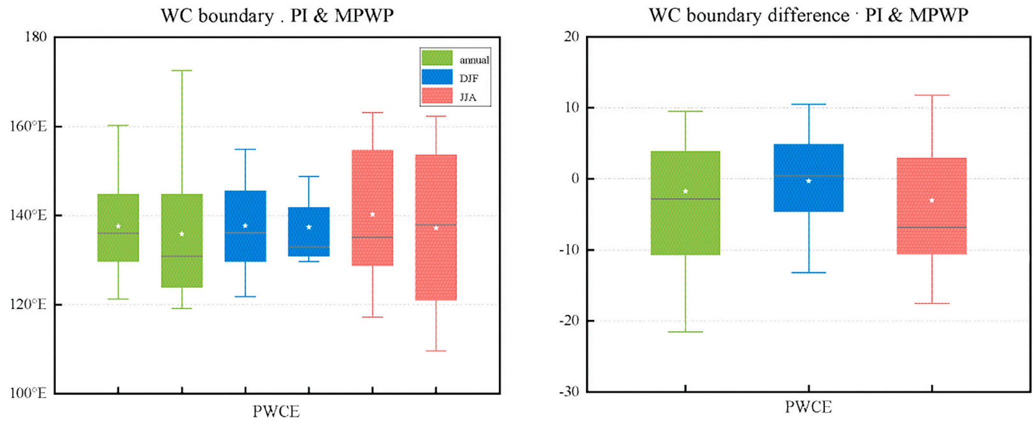

Fig. 4. Boxplots show the Western boundaries of PWC in two periods (left panel): PI and MPWP (left panel) and differences between MPWP and PI period (right panel). PWCE is the western edge of PWC.

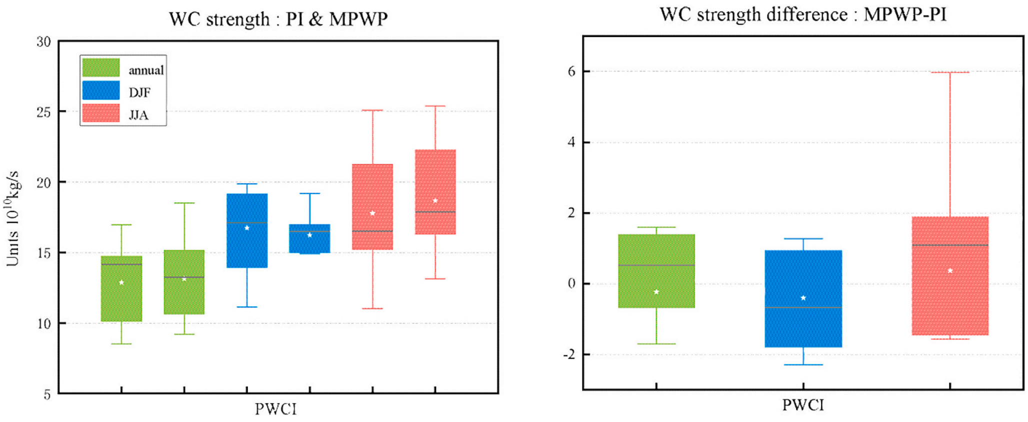

Fig. 5. Same as Fig. 2, except that boxplots show the strengths of PWC in two periods: PI and MPWP (left panel) and differences between MPWP and PI period (right panel). PWCI is the intensity of PWC.

$$\overline{v} = \frac{g}{2\pi a \cos\theta}\frac{\partial \psi}{\partial p} \tag{1}$$

$$\overline{\omega} = -\frac{g}{2\pi a \cos\theta}\frac{\partial \psi}{\partial \theta} \tag{2}$$

Where ψ is the MSF, the overbar indicates the latitude and time average, $\boldsymbol{g}$ is the Earth's gravitational acceleration, a is the mean Earth radius, and θ is the geographic latitude. Therefore, we can derive from equation (1) the expression of the mean meridional circulation via vertical integration of the zonal mean meridional velocity:

$$\psi = \frac{2\pi a \cos\theta}{g}\int_0^p \overline{v}\,dp \tag{3}$$

The vertical motion of the atmosphere can be decomposed into two parts: the meridional circulation and the latitudinal circulation (Nguyen

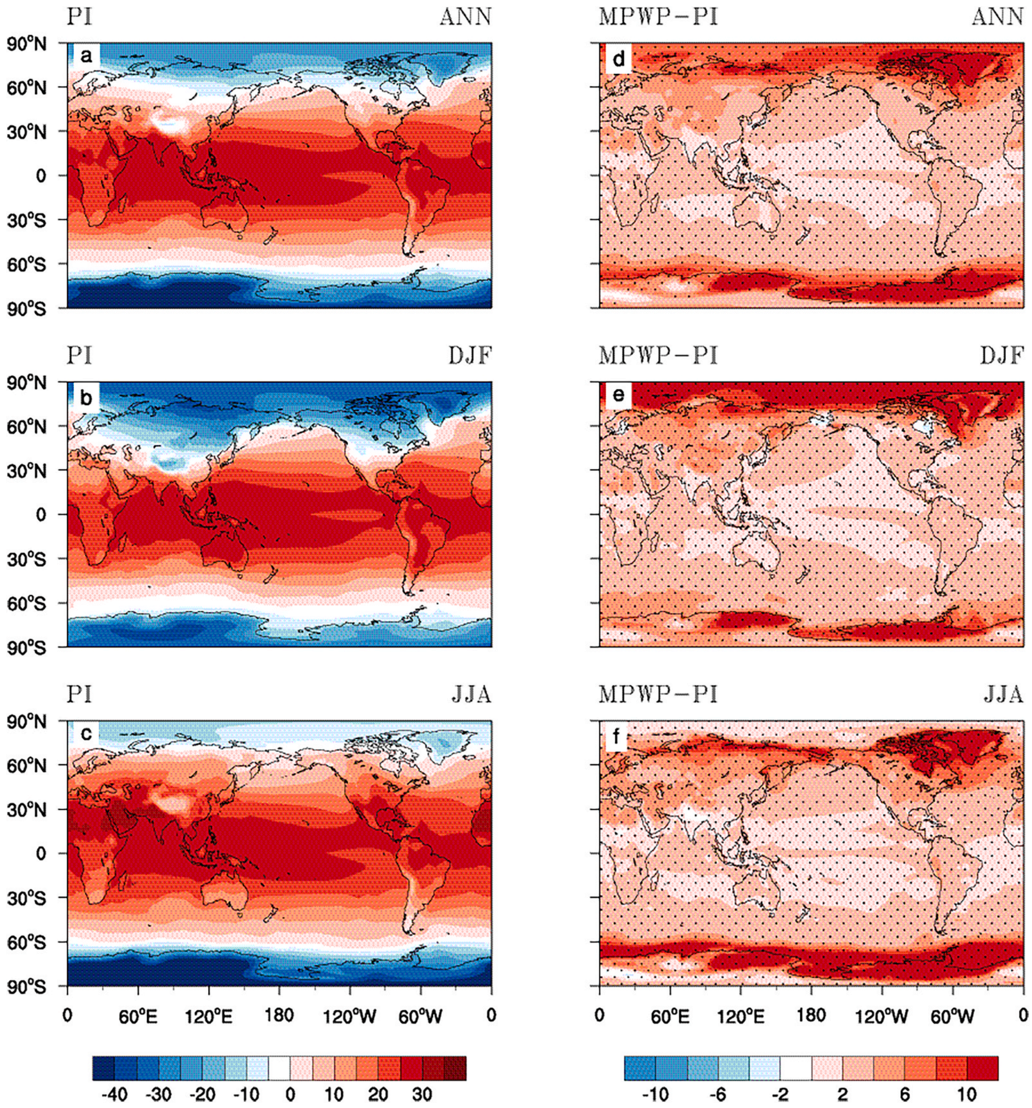

Fig. 6. Surface temperature (units: °C) in PI period in terms of annual mean (a), DJF (b) and JJA (c), and the changes of surface temperature in MPWP relative to PI in terms of annual mean (d), DJF (e) and JJA (f). Dotted areas indicate significant anomaly, MPWP-PI, at the 95% confidence interval.

et al., 2018; Schwendike et al., 2014). In consequence we can depict the Pacific Walker circulation (PWC) as a vertical integral of divergent components of the zonal winds:

$$\psi = \frac{2\pi a}{g} \int_0^p \overline{u}_d dp \tag{4}$$

Where u_d is the divergent component of the zonal wind.

2.2.2. *Definitions of positions and strengths of tropical atmospheric circulation*

The HC consists of the Hadley cell that spreads over latitude in both the Northern and Southern Hemispheres. The intensity of the Northern/Southern Hadley cell is defined as the maximum/minimum MSF in the Northern/Southern tropics (Feng et al., 2020; Sun et al., 2019; Hu et al., 2011, 2007; Oort and Yienger, 1996). The poleward extent limit of the HC is defined as the latitude where the amplitude of the MSF at 500 hPa equals zero in each hemisphere's subtropics (Sun et al., 2019; Hu et al., 2011; Hu and Fu, 2007).

The westward extent of the PWC is defined as the longitudinal position where the zonal stream function at 500 hPa is zero (Sun et al., 2013). Intensity of the tropical PWC is defined as the maximum zonal stream function between 120 °E and 90 °W.

2.2.3. *Tropical diabatic processes used to explain HC and WC changes*

In the tropics, the thermodynamic equation can be highly simplified to $Q \approx -\omega \times S_p$, where Q is diabatic heating (cooling), S_p is the stability parameter, and ω is the pressure velocity, representing the equilibrium between diabatic heating and upward adiabatic cooling of the air mass (Sohn et al., 2016). This form of the thermodynamic equation has been widely used in previous work to explain observed long-term trends in tropical circulation and projected future changes in tropical atmospheric circulation (Seo et al., 2014; Lu et al., 2007). However, it is not clear whether the simplified thermodynamic equations can describe the climatological upward and downward motions of the tropical atmospheric circulation, which is a prerequisite for explaining changes in the tropical circulation by changes in diabatic processes. Changes in static stability σ have typically been used to qualitatively understand changes in tropical circulation in previous studies (Mitas and Clement, 2006). Furthermore, the role of changes in static stability in changes in tropical atmospheric circulation is controversial (Chemke and Polvani, 2021; Seo et al., 2014; Mitas and Clement, 2006).

In this study, we first evaluate the mean diabatic processes of the tropical atmosphere using the simplified thermodynamic equations to examine the relationship between diabatic heating (cooling) and the rising (sinking) of the tropical atmospheric circulation. Then we

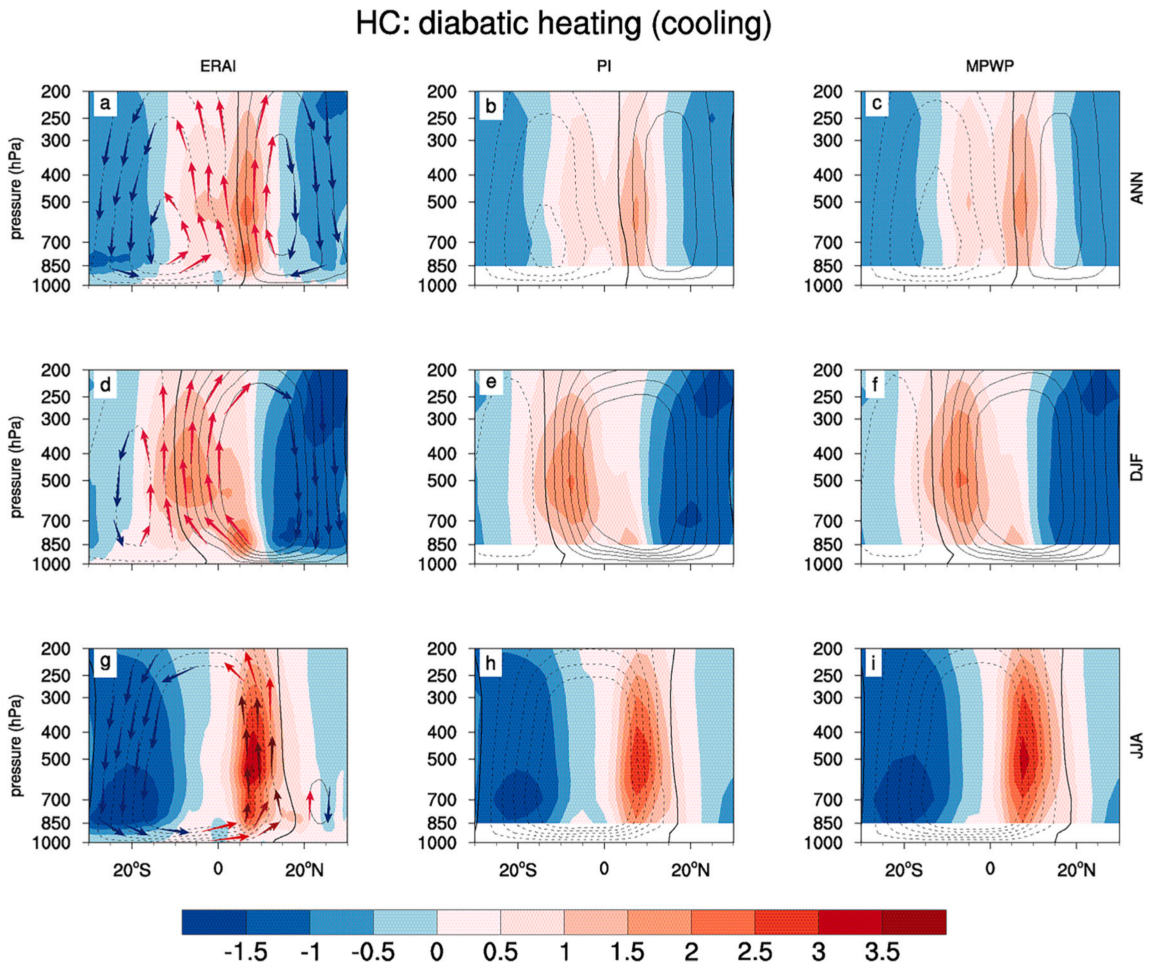

Fig. 7. The diabatic heating and cooling processes for ERAI, PI, and the MPWP (left to right, shaded, 10^{-5}K/s) compared to MSF (contours, 10^{10} kg/s) in terms of annual mean, DJF, JJA (top to bottom). The arrows in left panels schematically show the direction of HC.

decompose the changes in diabatic processes into the diabatic processes induced by the respective changes in S_p and ω i.e., $\dot{S_p} \times \omega$ (thermodynamic process) and $\dot{\omega} \times S_p$ (dynamical process). Thus we quantify the contribution of the two components to the tropical circulation changes during the MPWP.

3. Results

3.1. Generally weakened and widened HC with seasonal variation

We first examine the spatial distribution of the tropical atmospheric circulation response to MPWP surface warming based on the PlioMIP2 multi-model ensemble (MME) mean (pattern of individual model can be seen in Fig. S1), as changes in both the strength and boundary of the tropical atmospheric circulation depend on spatial patterns in the response. The HC consists of an ascending branch near the equator and a descending motion in the subtropics of both hemispheres (contours, Fig. 1a-b-c). Compared to PI (contours, Fig. 1a), the annual mean HC during the MPWP shows significant changes in the tropics and subtropics, manifested in an anomalous cross-equatorial counterclockwise circulation in the tropics (20°S∼20°N) and anomalous clockwise circulation in the northern subtropic (20°N∼40°N) (shaded, Fig. 1a).

The HC exhibits strong seasonality in terms of mean states and changes during the MPWP compared to PI (Fig. 1b and c). As for the mean state, HC is much stronger in the winter hemisphere than it is in the summer hemisphere (contours, Fig. 1b and c). Compared to PI, the Northern Hemisphere HC (NHC) and Southern Hemisphere HC (SHC) show different changes in boreal winter (DJF) during the MPWP, characterized by anomalous clockwise circulation in the SHC domain and south-to-north dipolar counterclockwise tropical circulation and clockwise subtropical circulation in the NHC domain (shaded, Fig. 1b). In contrast, a strong counterclockwise circulation anomaly occupies the area of SHC in boreal summer (JJA) during the MPWP, while the NHC in JJA during the MPWP shows clockwise and counterclockwise dipole structures in the upper and lower troposphere (shaded, Fig. 1c).

3.2. A westward shift and seasonally weakened PWC

The MME-based PI simulation can reasonably reproduce the observed features of annual, DJF, JJA mean PWC for the PI period, which is characterized by a rising branch in the tropical Indo-western Pacific and descending motion in the tropical eastern Pacific (Fig. 1d-e-f, contours). The response of the PWC to surface warming during the MPWP shows a spatially non-uniform distribution (pattern of individual model can be seen in Fig. S2). The annual mean stream function shows a triple response (from left to right, positive, negative, positive stream function anomalies; shaded in Fig. 1d). In contrast, PWC response to MPWP surface warming in DJF is characterized by negative, positive, negative stream function anomalies in Fig. 1e (left to right, shaded). In contrast to triple responses of PWC in annual and DJF, zonal dipole structure of PWC response to MPWP surface warming is observed in JJA, as manifested by narrow negative stream function anomalies on the left and broad positive stream function anomalies on the right (shaded, Fig. 1f). Spatially different responses of PWC among annual, DJF and

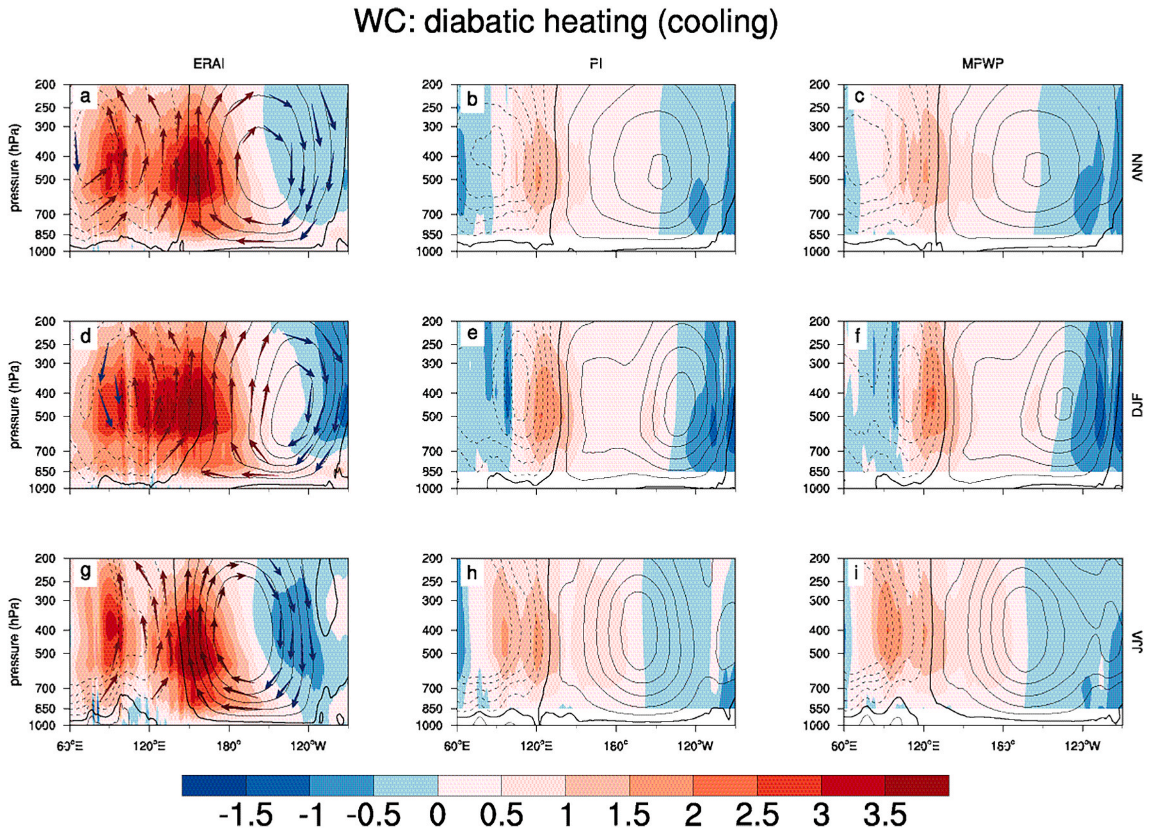

Fig. 8. Same as Fig. 7, except for diabatic heating and cooling processes compared to the stream function that represents PWC.

JJA lead to different behaviors of PWC intensity (PWCI) in annual, DJF and JJA during the MPWP (e.g., weakened PWCI in annual and DJF, enhanced PWCI in JJA). There is a statistically significant positive anomaly in the stream function in response to MPWP surface warming on the western side of the PWC in annual, DJF and JJA (clockwise circulation). These positive stream function anomalies push the edge of PWC toward the west in annual, DJF and JJA (Fig. 4b).

3.3. Mechanisms of tropical atmospheric circulation changes

Changes in meridional SST gradient and static stability S_p are two suggested processes to explain a poleward shift in the HC edges and a reduction in its strength (Chemke and Polvani, 2021; Carrapa et al., 2019; Adam et al., 2014; Seo et al., 2014; Kamae et al., 2011; Brierley et al., 2009; Mitas and Clement, 2006). Compared with PI period, the global mean surface air temperature during the MPWP show a polar amplification (Fig. 6), which also occurs in other research on the Pliocene (de Nooijer et al., 2020). This reduces the surface temperature gradient between the equator and pole, which could be a qualitative explanation for a weakened and widened HC during the MPWP. In addition, the increased static stability of the tropical atmosphere is another mechanism that qualitatively served to understand the reduced strength of the tropical atmospheric circulation (Fig. S3 and Fig. S4).

Nevertheless, in this study, we (1) used the diabatic heating and cooling processes and their comparison with ascending and descending motions of the tropical atmospheric circulation to quantify the changes in HC strength and PWC strength and the shift in the ascending branch of PWC. (2) Decomposition of changes in subtropic baroclinicity during the MPWP into contributions by changes in subtropical bulk static stability and by changes due to vertical wind shear changes.

3.3.1. Tropical diabatic processes and tropical atmospheric circulation

Given the HC and WC represent thermally direct circulation, a highly simplified thermodynamic equation is used to diagnose the large-scale behavior of HC and WC. Before evaluating the suitability of this dynamics analysis method for model simulations, we first used ERA-Interim reanalysis data obtained by assimilating conventional observations and satellite data (Berrisford et al., 2011) to investigate the spatial correspondence between diabatic processes and tropical atmospheric circulation motions over the observation period. In climatological conditions, the diabatic processes in ERAI spatially match well with the ascending and descending branches of HC and WC (Figs. 7 and 8), i.e., annual mean diabatic heating (cooling) in the tropics (subtropics) corresponds to the ascending (descending) motion (Fig. 7a). In addition, seasonality of diabatic heating/cooling processes coincides well with the seasonality of ascending/descending branch of HC in ERAI reanalysis (Fig. 7d and g). The simulated diabatic heating and cooling processes also agree well with the upward and downward motions of HC in the PI and MPWP periods (Fig. 7b-e-h; and c-f-i). The diabatic heating and cooling processes capture not only the large-scale feature of the HC, but also the rising and sinking branches of the PWC in the ERAI reanalysis and the simulations of the PI and MPWP periods (Fig. 8).

The definitions of the HC and PWC intensity depend on the spatial distributions of the response of the HC and PWC to warming. We therefore expect the changes in diabatic processes that are able to provide a further explanation for the spatial distribution of the HC and PWC responses, and thus enable us to use changes in diabatic processes to explain the changes in the strengths of the HC and PWC and the displacement of the PWC rising branch during the MPWP.

We firstly examine the changes in diabatic heating/cooling processes compared to the spatial distribution of the HC response during the MPWP. HC response to surface warming of the MPWP in the annual mean, DJF, and JJA is highly consist with changes in diabatic processes in the tropical atmosphere (Fig. 9a-d-g), i.e., anomalously rising airflow corresponds to anomalous diabatic heating (Fig. 9a-d-g, red shaded), and sinking airflow anomalies correspond to diabatic cooling anomalies

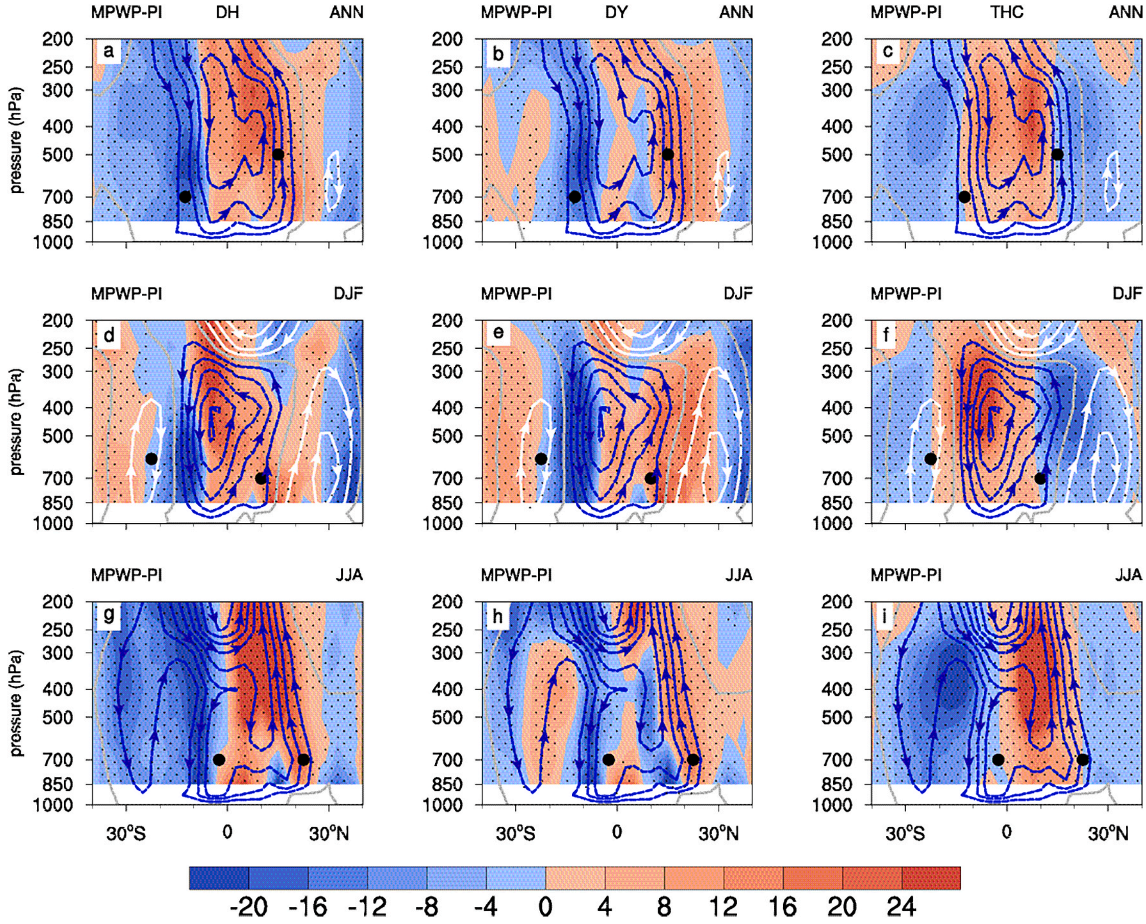

Fig. 9. The changes of diabatic heating/cooling processes (shaded, 10^{-7}K/s) compared to the changes of MSF (contours, 10^{10} kg/s) that represents HC. The changes of diabatic heating (cooling) in annual mean, DJF and JJA (a), (d), (j), respectively, contributed by the dynamic change (b), (e), (h) and the thermodynamic change (c), (f), (i) (shaded). The contours from top to bottom indicate MSF changes in MPWP relative to PI in the annual mean, DJF, and JJA, respectively. The dotted points indicate the location of the calculated HC intensity (i.e., maximum MSF value in the Northern Hemisphere and minimum MSF value in the Southern Hemisphere).

(Fig. 9a-d-g, blue shaded). The changes in diabatic processes are linearly decomposed into a contribution from changes in atmospheric circulation at constant static stability (dynamic contribution; Fig. 9b-e-h) and a contribution from changes in static stability at constant atmospheric circulation (thermodynamic contribution; Fig. 9c-f-i), as described in Section 2.2.3. Changes in tropical diabatic processes in the annual and DJF during the MPWP are mainly due to the dynamical contribution (Fig. 9a and b; d-e), while the thermodynamic contribution is opposite to the changes in diabatic heating and cooling in the annual and DJF during the MPWP (Fig. 9a–c; 9 d-f). In contrast, the changes in diabatic processes in JJA during the MPWP result from the combined effects of thermodynamic and dynamical contributions (Fig. 9g-h-i).

As NHCI (Northern Hadley circulation Intensity) weakens in the annual mean, DJF and JJA, and SHCI (Southern Hadley circulation Intensity) increases in the annual mean and JJA while weakening in the DJF (Fig. 2b), this reflects the changes in different diabatic processes that contribute to seasonal changes in NHCI and SHCI (Fig. 9). Changes in diabatic processes due to the dynamic contribution lead to a weakening of the NHCI during the MPWP in the annual, DJF, JJA (Fig. 9b-e-h). In contrast, the dynamic and thermodynamic contributions to the changes in diabatic processes strengthen the SHCI during the MPWP in annual and JJA, respectively (Fig. 9b–i), while the weakening of the SHCI in the JJA is mainly due to the changes in the diabatic processes caused by dynamic contribution (Fig. 9e).

Similarly, the changes in diabatic heating and cooling processes are well matched to the rise and sink branches of the PWC anomalies during the MPWP (Fig. 10a-d-g). i.e., anomalous diabatic heating (cooling) corresponds to anomalous rising (sinking) motion. The weakening of PWCI during the MPWP in both annual and DJF is a result of changes in diabatic heating and cooling processes due to dynamic contribution (Fig. 5b and Fig. 10b-e); while the enhanced PWCI during the MPWP in JJA is due to changes in diabatic heating and cooling processes changes due to thermodynamic contribution (Figs. 5b and 10i). In addition, the rising and sinking anomalies triggered by the anomalous diabatic heating of the atmosphere in the western part of the tropical Indian Ocean and the anomalous diabatic cooling of the atmosphere in the eastern part of the tropical Indian Ocean formed a clockwise circulation that shifted the rising branch of the PWC (PWCE) westward (Fig. 10a-d-g and Fig. 4b). The changes in diabatic processes in the atmosphere of the tropical Indian Ocean are mainly due to the contribution of dynamical processes (Fig. 10d-e-h). Therefore, it is the dynamical processes that lead to the westward shift of the ascending branch of the PWC during the MPWP (Fig. 4b).

3.3.2. *Subtropical baroclinicity and HC edges*

In this section, we explain the shift of the margins of HC and PWC by the tropical-subtropical diabatic processes together with the subtropical baroclinicity. As an important factor affecting subtropical baroclinicity, the increase (decrease) in bulk static stability in the subtropics leads to a weakening (strengthening) of subtropical baroclinicity, which explains the widening (shrinking) of HC (in the boreal summer) during the MPWP (Fig. 11). As another important factor affecting subtropical baroclinicity, the contribution of changes in subtropical baroclinicity caused by changes in subtropical vertical shear of the zonal wind to the

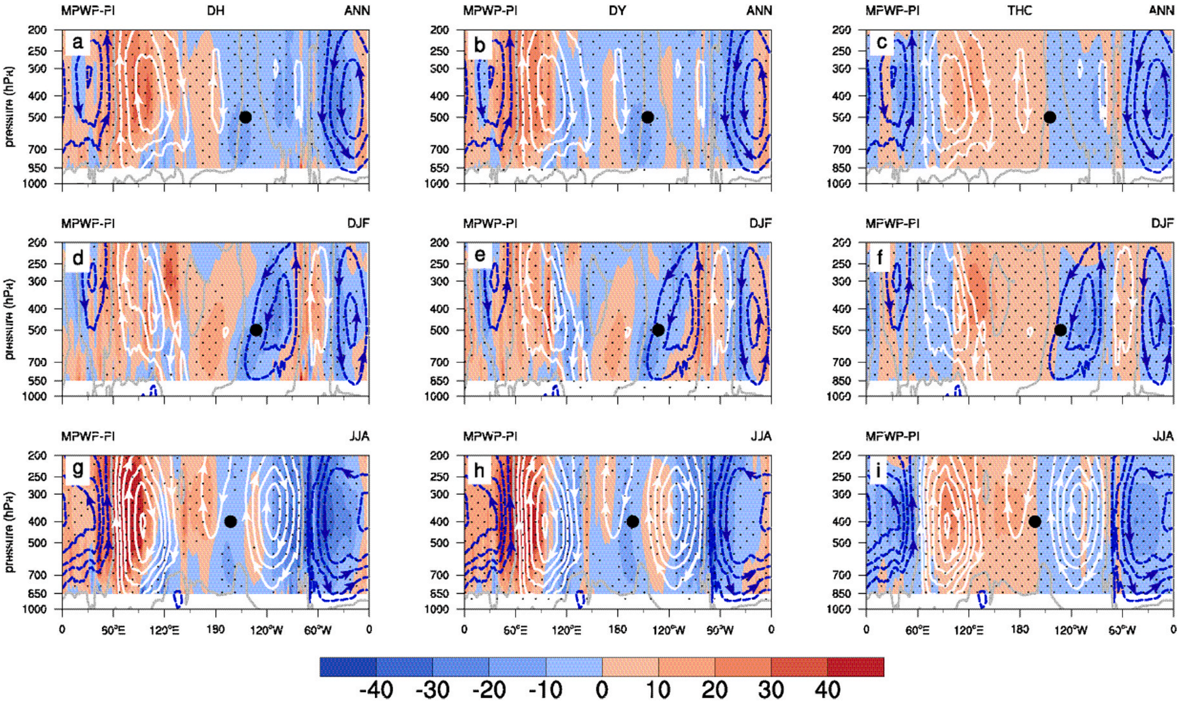

Fig. 10. Same as Fig. 9, except for the changes of diabatic heating (cooling) compared to the changes of stream function that represents PWC. The dotted points indicate the location of the calculated stream function intensity (i.e., maximum value). These results are obtained by averaging over the latitudinal band 30°S~30°N.

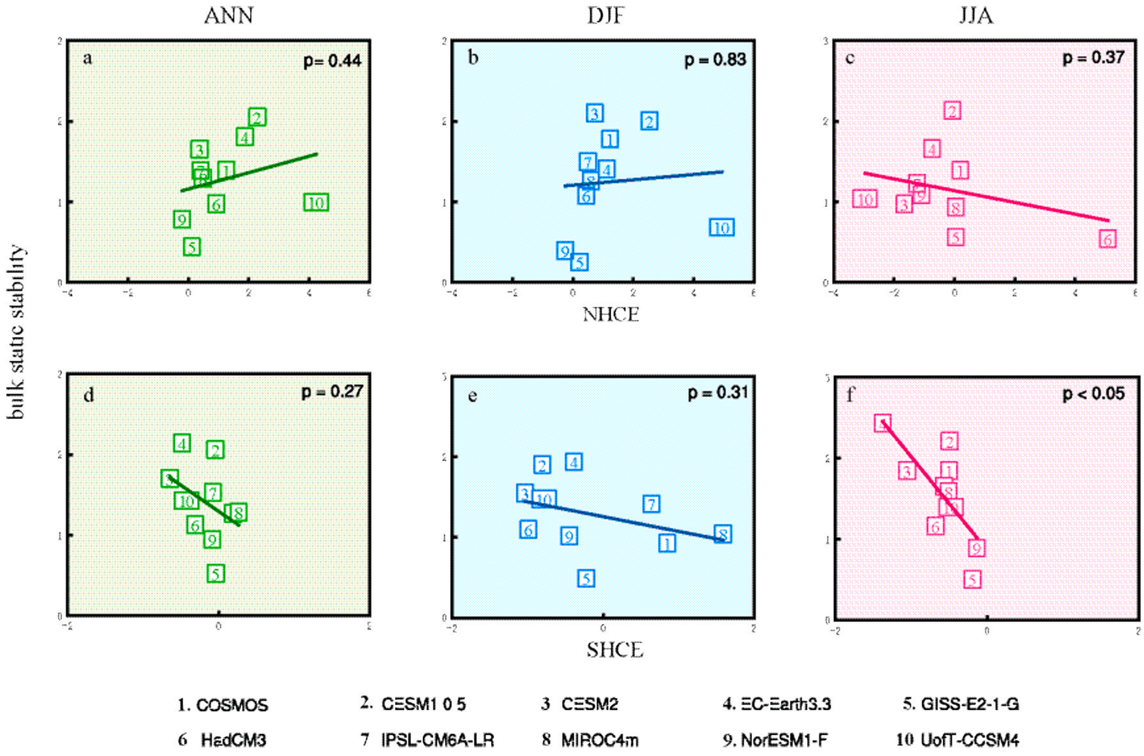

Fig. 11. Scatter plots showing the relationship between changes in HC edges and changes in bulk static stability in the Northern (top) and Southern (bottom) Hemispheres for annual mean, DJF, JJA respectively (from left to right). The dashed line in each figure is the linear regression between the two. Following the work of Kim, the bulk static stability $\theta_z = (\theta_{500} - \theta_{850})$ and the vertical wind shear $u_z = (u_{500} - u_{850})$ are two factors that affect the baroclinicity $C \equiv \frac{f^2 u_z}{\beta g H \theta_z/\theta_0}$, f, β, g, H, and Θ_0 are Coriolis parameter, latitudinal gradient, gravitational acceleration, depth scale, and reference potential temperature (Kim et al., 2023).

shift in the HC edges, however, varies seasonally (Fig. 12). There is a negative (positive) correlation between the change in the annual NHCE (SHCE) and the change in the annual vertical wind shear of the subtropical wind in the northern (southern) hemisphere, i.e., the decrease in the vertical wind shear in the northern and southern subtropics leads to the expansion of the HC by decreasing the subtropical

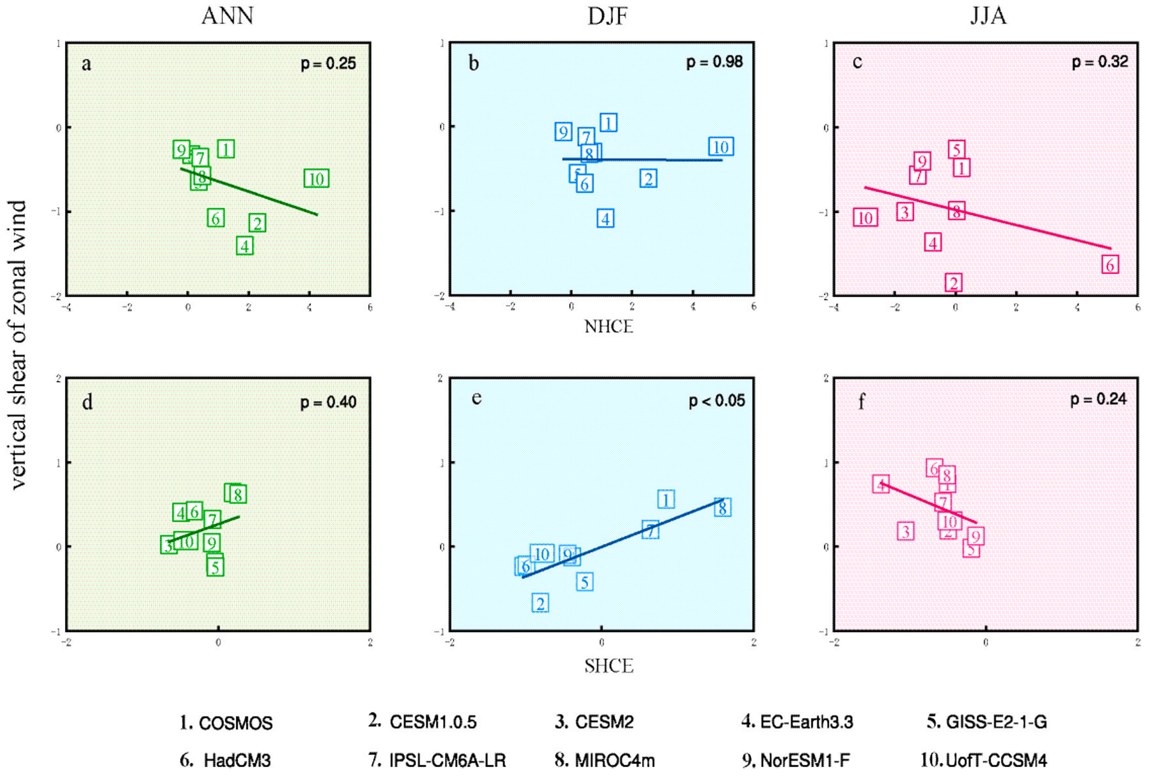

Fig. 12. Same as Fig. 11, except showing the changes in HC edge versus the changes in the vertical shear of the zonal wind u_z.

baroclinicity in both subtropics during the MPWP (Fig. 12a–d). A similar positive correlation between the SHCE changes and the changes in the vertical shear of the subtropical winds in the Southern Hemisphere exists in boreal winter, yet there is no correlation between the NHCE changes and the changes in the vertical shear of the subtropical winds in the Northern Hemisphere in boreal winter (Fig. 12b–e). This suggests that changes in subtropical vertical wind shear during the MPWP that favor the poleward expansion of SHCE in boreal winter (Fig. 12b) but contribute insignificantly to the shift in NHCE in boreal winter (Fig. 12e). Unlike the relationship in boreal winter, subtropical vertical wind shear in the northern and southern hemispheres is negatively correlated with the NHCE and SHCE in boreal summer. However, this negative correlation shows that the changes in subtropical baroclinicity caused by the changes in subtropical vertical wind shear in the northern and southern subtropics tend to expand the NHCE and shrink the SHCE, respectively, which contrasts with the changes in the NHCE and shrink the SHCE during the MPWP (Fig. 3b).

Anomalies in MSF during the MPWP associated with the changes in diabatic processes from the tropics to the subtropics can also be used to explain the shift in the HC edges during the MPWP. For example, the clockwise circulation anomalies in the Northern Hemisphere caused by tropical heating and extratropical cooling can explain the poleward shift of the northern limit of the HC in annual, DJF during the MPWP (Fig. 9a–d; Fig. 3b). The poleward shift of the southern limit of the HC (SHCE) in annual and JJA can be explained by the anti-clockwise circulation anomalies in the Southern Hemisphere due to tropical heating and extratropical cooling (Fig. 9a–g; Fig. 3b). In addition, anomalous clockwise zonal circulation (60°E−180) mainly due to tropical heating (30°E−90°E) contributes to a westward shift of the PWCE in annual, DJF and JJA during the MPWP (Fig. 10a-d-g; Fig. 4b).

4. Summary and conclusions

In this study, we have examined the changes in tropical atmospheric circulation (HC and PWC) and associated mechanism in a geologic warm period (MPWP) that approximates future scenarios by using 12 climate models participating in PlioMIP2. We then focused on the changes in tropical atmospheric circulation intensity and boundary shift and emphasized that the diabatic heating/cooling processes can be used as a new perspective to explain the changes in intensity of HC and PWC as well as PWC shift. Our key findings are summarized as follows.

(1) HC and PWC changes:

Compared with the PI period, the intensity of the HC during the MPWP is characterized by (1) differences in the changes of HC between the Northern and Southern Hemispheres and (2) apparent seasonality of HC changes even in the same hemisphere. In contrast to the consistent weakening of NHCI and SHCI in the DJF, annual and JJA SHCI are increased during the MPWP. Unlike a seasonally consistent weakening of the NHCI, SHCI weakens in DJF but strengthens in JJA. Similarly, unlike the consistently poleward expansion of the SHCE, the poleward expansion of NHCE during the MPWP is observed in annual and DJF, but it shrinks in JJA.

The PWCI weakens in DJF and strengthens in JJA as does the apparent seasonality of the SHCI during the MPWP, while the PWCE during the MPWP moves consistently westward in annual, DJF, JJA.

(2) Tropical diabatic processes explain the changes of HC and PWC strength

The tropical diabatic processes are not only good at representing the upward and downward motion of the tropical atmospheric circulation, but their changes also agree well with the spatial distribution of the upward and downward motion changes of the tropical atmospheric circulation. i.e., diabatic heating corresponds to rising and conversely to sinking. Thus, we mechanistically explain changes in weakening of NHCI (in annual, DJF, JJA), SHCI (DJF) and PWCI (annual, DJF) and strengthening of SHCI (annual, JJA) and PWCI (JJA), and westward shift of the PWC ascending branch (annual, DJF, JJA) during the MPWP by diagnosing changes in diabatic processes.

(3) Decrease in subtropical baroclinicity shifts the HC edges poleward

Increase and decrease in the subtropical bulk static stability in the Northern Hemisphere expand (annual, DJF) and contract (JJA) the NHCE by suppressing and increasing the subtropical baroclinicity of the atmosphere, respectively. Meanwhile, the poleward expansion of the SHCE mainly arises from the weakened subtropical baroclinicity due to the increase static stability of the subtropical atmosphere in the Southern Hemisphere.

Changes in vertical shear in the subtropical zonal winds during the MPWP contribute to changes in the HC boundary by altering the subtropical baroclinicity, but their role varies seasonally.

Author contributions

Ke Zhang: Writing - original draft, dynamic analysis. Yong Sun: Conceptualization, methodology. Zhongshi Zhang: Data supply for model NorESM-F. Christian Stepanek: Data supply for model COSMOS. Ran Feng: Data supply for model CESM2, Writing - review & editing. Daniel Hill: Writing - review & editing. Gerrit Lohmann: Data supply for model COSMOS. Aisling Dolan: Data supply for model HadCM3. Alan Haywood: Data supply for model HadCM3. Ayako Abe-Ouchi: Data supply for model MIROC4m. Bette Otto-Bliesner: Data supply for model CESM2. Camille Contoux: Data supply for model IPSL-CM6A-LR and IPSL-CM5A. Deepak Chandan: Data supply for model UofT-CCSM4. Gilles Ramstein: Data supply for model IPSL-CM6A-LR, IPSL-CM5A2.1, and IPSL-CM5A. Harry Dowsett: Data supply for PRISM4 boundary conditions. Julia Tindall: Data supply for model HadCM3. Michiel Baatsen: Data supply for model CESM 1.0.5. Ning Tan: Data supply for model IPSL-CM5A2.1. William Richard Peltier: Data supply for model UofT-CCSM4. Qiang Li: Data supply for model EC-Earth 3.3. Wing-Le Chan: Data supply for model MIROC4m. Xin Wang: Writing - review & editing. Xu Zhang: Conceptualization, funding acquisition.

Data availability

All data discussed are presented in the manuscript or in the Supplementary table.

Declaration of competing interest

We confirm that all co-authors are aware of this submission and declare that the material presented here is the result of our own work, and has not been submitted to any other journal, or published elsewhere. The authors declare that they have no conflict of interest.

Acknowledgments

This study is supported by the National Key Research and Development Program (2020YFA0608902) and National Science Foundation of China (no. 42075047).

Funding for HD was provided by the U.S. Geological Survey Climate R&D Program. Any use of trade, firm, or product names is for descriptive purposes only and does not imply endorsement by the U.S. Government.

The CESM2 simulations are performed with high-performance computing support from Cheyenne (https://doi.org/10.5065/D6RX99HX) provided by NCAR's Computational and Information Systems Laboratory, sponsored by the National Science Foundation. RF acknowledges support from National Science Foundation (No. 2103055).

Gerrit Lohmann and Christian Stepanek acknowledge institutional funding from the Alfred Wegener Institute (AWI) via the research programme PACES-II of the Helmholtz Association. Christian Stepanek acknowledges funding from the Helmholtz Climate Initiative REKLIM.

Bette Otto-Bliesner acknowledges support by the National Center for Atmospheric Research, which is a major facility sponsored by the National Science Foundation under Cooperative Agreement No. 1852977.

Appendix A. Supplementary data

Supplementary data to this article can be found online at https://doi.org/10.1016/j.quaint.2024.01.001.

References

Adam, O., Schneider, T., Harnik, N., 2014. Role of changes in mean temperatures versus temperature gradients in the recent widening of the Hadley circulation. J. Clim. 27 (19), 7450–7461. https://doi.org/10.1175/JCLI-D-14-00140.1.

Baatsen, M.L., von der Heydt, A.S., Kliphuis, M.A., et al., 2021. Warm mid-Pliocene conditions without high climate sensitivity: the CCSM4-Utrecht (CESM 1.0.5) contribution to the PlioMIP2. Clim. Past 18, 657–679. https://doi.org/10.5194/cp-18-657-2022.

Bartoli, G., Hönisch, B., Zeebe, R.E., 2011. Atmospheric CO2 decline during the Pliocene intensification of northern hemisphere glaciations. Paleoceanography 26 (4), PA4213. https://doi.org/10.1029/2010PA002055.

Berntell, E., Zhang, Q., Li, Q., et al., 2021. Mid-pliocene west african monsoon rainfall as simulated in the Pliomip2 ensemble. Clim. Past 17 (4), 1777–1794. https://doi.org/10.5194/cp-17-1777-2021.

Berrisford, P., Kållberg, P., Kobayashi, S., Dee, D., Uppala, S., Simmons, A.J., Poli, P., Sato, H., 2011. Atmospheric conservation properties in ERA-Interim. Q. J. R. Meteorol. Soc. 137, 1381–1399. https://doi.org/10.1002/qj.864.

Brierley, C.M., Fedorov, A.V., Liu, Z., et al., 2009. Greatly expanded tropical warm pool and weakened Hadley circulation in the early Pliocene. Science 323 (5922), 1714–1718. https://doi.org/10.1126/science.1167625.

Burke, K.D., Williams, J.W., Chandler, M.A., et al., 2018. Pliocene and Eocene provide best analogs for near-future climates. Proc. Natl. Acad. Sci. USA 115 (52), 13288–13293. https://doi.org/10.1073/pnas.1809600115.

Carrapa, B., Clementz, M., Feng, R., 2019. Ecological and hydroclimate responses to strengthening of the Hadley circulation in South America during the Late Miocene cooling. Proc. Natl. Acad. Sci. 116, 9747–9752. https://doi.org/10.1073/pnas.1810721116.

Chan, W.-L., Abe-Ouchi, A., 2020. Pliocene model intercomparison project (PlioMIP2) simulations using the model for interdisciplinary research on climate (MIROC4m). Clim. Past 16 (4), 1523–1545. https://doi.org/10.5194/cp-16-1523-2020.

Chandan, D., Peltier, W.R., 2018. On the mechanisms of warming the mid-Pliocene and the inference of a hierarchy of climate sensitivities with relevance to the understanding of climate futures. Clim. Past 14 (6), 825–856. https://doi.org/10.5194/cp-14-825-2018.

Chandler, M., Rind, D., Thompson, R., 1994. Joint investigations of the middle Pliocene climate II: GISS GCM Northern Hemisphere results. Global Planet. Change 9 (3–4), 197–219. https://doi.org/10.1016/0921-8181(94)90016-7.

Chandler, M.A., Sohl, L.E., Jonas, J.A., et al., 2013. Simulations of the mid-pliocene Warm Period using two versions of the NASA/GISS ModelE2-R coupled model. Geosci. Model Dev. (GMD) 6 (2), 517–531. https://doi.org/10.5194/gmd-6-517-2013.

Chemke, R., Polvani, L.M., 2021. Elucidating the mechanisms responsible for Hadley cell weakening under 4×CO2 forcing. Geophys. Res. Lett. 48 (3), e2020GL090348 https://doi.org/10.1029/2020GL090348.

Contoux, C., Ramstein, G., Jost, A., 2012. Modelling the mid-Pliocene Warm Period climate with the IPSL coupled model and its atmospheric component LMDZ5A. Geosci. Model Dev. (GMD) 5 (3), 903–917. https://doi.org/10.5194/gmd-5-903-2012.

Cook, K.H., 2003. Role of continents in driving the Hadley cells. J. Atmos. Sci. 60 (7), 957–976.

Corvec, S., Fletcher, C.G., 2017. Changes to the tropical circulation in the mid-Pliocene and their implications for future climate. Clim. Past 13 (2), 135–147. https://doi.org/10.5194/cp-13-135-2017.

Danabasoglu, G, Bates, S C, Briegleb, B P, et al., 2012. The CCSM4 ocean component. J. Clim. 25 (5), 1361–1389. https://doi.org/10.1175/JCLI-D-11-00091.1.

Danabasoglu, G, Lamarque, J F, Bacmeister, J, et al., 2020. The community earth system model version 2 (CESM2). J. Adv. Modeling Earth Syst. 12 (2) e2019MS001916. https://doi.org/10.1029/2019MS001916.

de Nooijer, W., Zhang, Q., Li, Q., et al., 2020. Evaluation of arctic warming in mid-pliocene climate simulations. Clim. Past 16 (6), 2325–2341. https://doi.org/10.5194/cp-16-2325-2020.

Dowsett, H.J., Thompson, R., Barron, J., et al., 1994. Joint investigations of the Middle Pliocene climate I: PRISM paleoenvironmental reconstructions. Global Planet. Change 9 (3–4), 169–195. https://doi.org/10.1016/0921-8181(94)90015-9.

Dowsett, H.J., Barron, J.A., Poore, R.Z., et al., 1999. Middle Pliocene paleoenvironmental reconstruction: PRISM2. US Geol. Surv. open file Rep. 99 (535), 236. https://doi.org/10.3133/ofr99535.

Dowsett, H.J., Haywood, A.M., Valdes, P.J., et al., 2011. Sea surface temperatures of the mid-piacenzian Warm Period: a comparison of PRISM3 and HadCM3. Palaeogeogr. Palaeoclimatol. Palaeoecol. 309 (1–2), 83–91. https://doi.org/10.1016/j.palaeo.2011.03.016.

Dowsett, H.J., Robinson, M.M., Stoll, D.K., et al., 2013. The PRISM (Pliocene palaeoclimate) reconstruction: time for a paradigm shift. Phil. Trans. Math. Phys. Eng. Sci. 371 (2001), 20120524 https://doi.org/10.1098/rsta.2012.0524.

Dowsett, H., Dolan, A., Rowley, D., et al., 2016. The PRISM4 (Mid-Piacenzian) paleoenvironmental reconstruction. Clim. Past 12 (7), 1519–1538. https://doi.org/10.5194/cp-12-1519-2016.

Feng, J., Zhu, J., Li, F., 2016. Climatological vertical features of Hadley circulation depicted by the NCEP/NCAR, ERA40, NCEP-DOE, JRA25, ERA-Interim, and CFSR reanalyses. Sola 12, 237–241. https://doi.org/10.2151/sola.2016-047.

Feng, J., Li, J., Zhu, J., et al., 2015. Simulation of the equatorially asymmetric mode of the Hadley circulation in CMIP5 models. Adv. Atmos. Sci. 32, 1129–1142. https://doi.org/10.1007/s00376-015-4157-0.

Feng, R., Bhattacharya, T., Otto-Bliesner, B.L., et al., 2022. Past terrestrial hydroclimate sensitivity controlled by Earth system feedbacks. Nat. Commun. 13 (1), 1306. https://doi.org/10.1038/s41467-022-28814-7.

Feng, R., Otto-Bliesner, B.L., Brady, E.C., et al., 2020. Increased climate response and Earth system sensitivity from CCSM4 to CESM2 in mid-pliocene simulations. J. Adv. Model. Earth Syst. 12 (8), E2019MS002033 https://doi.org/10.1029/2019ms002033.

Gordon, C, Cooper, C, Senior, C A, et al., 2000. The simulation of SST, sea ice extents and ocean heat transports in a version of the Hadley Centre coupled model without flux adjustments. Clim. Dyn. 16, 147–168.

Han, Z., Zhang, Q., Li, Q., et al., 2021. Evaluating the large-scale hydrological cycle response within the Pliocene model Intercomparison project Phase 2 (PlioMIP2) ensemble. Clim. Past 17 (6), 2537–2558. https://doi.org/10.5194/cp-17-2537-2021.

Haywood, A.M., Valdes, P.J., Sellwood, B.W., 2000. Global scale palaeoclimate reconstruction of the middle Pliocene climate using the UKMO GCM: initial results. Global Planet. Change 25 (3–4), 239–256. https://doi.org/10.1016/S0921-8181(00)00028-X.

Haywood, A.M., Hill, D.J., Dolan, A.M., et al., 2013. Large-scale features of Pliocene climate: results from the Pliocene model Intercomparison project. Clim. Past 9 (1), 191–209. https://doi.org/10.5194/cp-9-191-2013.

Haywood, A.M., Dowsett, H.J., Dolan, A.M., et al., 2016. The Pliocene model Intercomparison project (PlioMIP) Phase 2: scientific objectives and experimental design. Clim. Past 12 (3), 663–675. https://doi.org/10.5194/cp-12-663-2016.

Haywood, A.M., Tindall, J.C., Dowsett, H.J., et al., 2020. The Pliocene model Intercomparison project Phase 2: large-scale climate features and climate sensitivity. Clim. Past 16 (6), 2095–2123. https://doi.org/10.5194/cp-16-2095-2020.

Haywood, A.M., Dowsett, H.J., Tindall, J.C., et al., 2021. PlioMIP1 and PlioMIP2 participants. PlioMIP: the Pliocene model Intercomparison project. Past Glob. Changes Magazine 29 (2), 92–93. https://doi.org/10.22498/pages.29.2.92.

Hopcroft, P.O., Ramstein, G., Pugh, T.A., et al., 2020. Polar amplification of Pliocene climate by elevated trace gas radiative forcing. Proc. Natl. Acad. Sci. USA 117 (38), 23401–23407. https://doi.org/10.1073/pnas.2002320117.

Hourdin, F, Rio, C, Grandpeix, J Y, et al., 2020. LMDZ6A: The atmospheric component of the IPSL climate model with improved and better tuned physics. J. Adv. Modeling Earth Syst. 12 (7) e2019MS001892. https://doi.org/10.1029/2019MS001892.

Hu, S., Chou, J., Cheng, J., 2018. Three-pattern decomposition of global atmospheric circulation: part I—decomposition model and theorems. Clim. Dynam. 50 (1–2), 2355–2368. https://doi.org/10.1007/s00382-015-2818-4.

Hu, Y., Fu, Q., 2007. Observed poleward expansion of the Hadley circulation since 1979. Atmos. Chem. Phys. 7 (19), 5229–5236. https://doi.org/10.5194/acp-7-5229-2007.

Hu, Y., Zhou, C., Liu, J., 2011. Observational evidence for poleward expansion of the Hadley circulation. Adv. Atmos. Sci. 28, 33–44. https://doi.org/10.1007/s00376-010-0032-1.

Hu, Y., Tao, L., Liu, J., 2013. Poleward expansion of the Hadley circulation in CMIP5 simulations. Adv. Atmos. Sci. 30, 790–795. https://doi.org/10.1007/s00376-012-2187-4.

Hunter, S.J., Haywood, A.M., Dolan, A.M., et al., 2019. The Hadcm3 contribution to pliomip Phase 2. Clim. Past 15, 1691–1713. https://doi.org/10.5194/cp-15-1691-2019.

Jansen, E., Overpeck, J., Briffa, K.R., et al., 2007. Palaeoclimate. In: Solomon, S., Qin, D., Manning, M., Chen, Z., Marquis, M., Averyt, K.B., Tignor, M., Miller, H.L. (Eds.), Climate Change 2007: the Physical Science Basis. Contribution of Working Group I to the Fourth Assessment Report of the Intergovernmental Panel on Climate Change. Cambridge University Press, pp. 433–497.

Kamae, Y., Ueda, H., Kitoh, A., 2011. Hadley and Walker circulations in the mid-Pliocene warm period simulated by an atmospheric general circulation model. J. Meteorol. Soc. Japan. Ser. II. 89 (5), 475–493. https://doi.org/10.2151/jmsj.2011-505.

Kamae, Y., Yoshida, K., Ueda, H., 2016. Sensitivity of Pliocene climate simulations in MRI-CGCM2. 3 to respective boundary conditions. Clim. Past 12 (8), 1619–1634. https://doi.org/10.5194/cp-12-1619-2016.

Kelley, M, Schmidt, G A, Nazarenko, L S, et al., 2020. GISS-E2. 1: Configurations and climatology. J. Adv. Modeling Earth Syst. 12 (8) e2019MS002025. https://doi.org/10.1029/2019MS002025.

Kim, S.Y., Choi, Y.J., Son, S.W., et al., 2023. Hemispherically asymmetric Hadley cell response to CO_2 removal. Sci. Adv. 9 (30), eadg1801 https://doi.org/10.1126/sciadv.adg1801.

Li, X., Guo, C., Zhang, Z., et al., 2020. PlioMIP2 simulations with NorESM-L and NorESM1-F. Clim. Past 16 (1), 183–197. https://doi.org/10.5194/cp-16-183-2020.

Lu, J., Vecchi, G.A., Reichler, T., 2007. Expansion of the Hadley cell under global warming. Geophys. Res. Lett. 34 (6), L06805 https://doi.org/10.1029/2006GL028443.

Lunt, D.J., Haywood, A.M., Schmidt, G.A., et al., 2010. Earth system sensitivity inferred from Pliocene modelling and data. Nat. Geosci. 3 (1), 60–64. https://doi.org/10.1038/ngeo706.

Lurton, T., Balkanski, Y., Bastrikov, V., et al., 2020. Implementation of the CMIP6 forcing data in the IPSL-cm6a-LR model. J. Adv. Model. Earth Syst. 12 (4), e2019MS001940 https://doi.org/10.1029/2019MS001940.

Madec, G., 2008. NEMO ocean engine, (Vol. 27).. Institut Piere-Simon Laplace (IPSL, France.

Madec, G., Bourdallé-Badie, R., Bouttier, P. A., et al., 2017. NEMO ocean engine.

Madec, G, Imbard, M. A, 1996. global ocean mesh to overcome the North Pole singularity. Clim. Dyn. 12, 381–388. https://doi.org/10.1007/BF00211684.

Martínez-Botí, M.A., Foster, G.L., Chalk, T.B., et al., 2015. Plio-Pleistocene climate sensitivity evaluated using high-resolution CO_2 records. Nature 518 (7537), 49–54. https://doi.org/10.1038/nature14145.

McClymont, E.L., Ford, H.L., Ho, S.L., et al., 2020. Lessons from a high-CO_2 world: an ocean view from ~3 million years ago. Clim. Past 16 (4), 1599–1615. https://doi.org/10.5194/cp-16-1599-2020.

Mitas, C.M., Clement, A., 2006. Recent behavior of the Hadley cell and tropical thermodynamics in climate models and reanalyses. Geophys. Res. Lett. 33 (1), L01810 https://doi.org/10.5194/cp-16-1599-2020.

Neale, R B, Chen, C C, Gettelman, A, et al., 2010. Description of the NCAR community atmosphere model (CAM 5.0). NCAR Tech. Note NCAR/TN-486+ STR 1 (1), 1–12.

Nguyen, H., Hendon, H.H., Lim, E.P., et al., 2018. Variability of the extent of the Hadley circulation in the southern hemisphere: a regional perspective. Clim. Dynam. 50, 129–142. https://doi.org/10.1007/s00382-017-3592-2.

Oort, A.H., Yienger, J.J., 1996. Observed interannual variability in the Hadley circulation and its connection to ENSO. J. Clim. 9 (11), 2751–2767. http://www.jstor.org/stable/26201418.

Pagani, M., Liu, Z., LaRiviere, J., et al., 2010. High Earth-system climate sensitivity determined from Pliocene carbon dioxide concentrations. Nat. Geosci. 3 (1), 27–30. https://doi.org/10.1038/ngeo724.

Peltier, W.R., Vettoretti, G., 2014. Dansgaard-Oeschger oscillations predicted in a comprehensive model of glacial climate: a "kicked" salt oscillator in the Atlantic. Geophys. Res. Lett. 41 (20), 7306–7313. https://doi.org/10.1002/2014GL061413.

Pope, V D, Gallani, M L, Rowntree, P R, et al., 2000. The impact of new physical parametrizations in the Hadley Centre climate model. HadAM3. Clim. Dyn. 16, 123–146. https://doi.org/10.1007/s003820050009.

Pound, M.J., Tindall, J., Pickering, S.J., et al., 2014. Late Pliocene lakes and soils: a global data set for the analysis of climate feedbacks in a warmer world. Clim. Past 10 (1), 167–180. https://doi.org/10.5194/cp-10-167-2014.

Roeckner E, Bäuml G, Bonaventura L, et al., 2003. The atmospheric general circulation model ECHAM 5. PART I: Model description.

Salzmann, U., Dolan, A.M., Haywood, A.M., et al., 2013. Challenges in quantifying Pliocene terrestrial warming revealed by data–model discord. Nat. Clim. Change 3 (11), 969–974. https://doi.org/10.1038/nclimate2008.

Schwendike, J., Govekar, P., Reeder, M.J., et al., 2014. Local partitioning of the overturning circulation in the tropics and the connection to the Hadley and Walker circulations. J. Geophys. Res. Atmos. 119 (3), 1322–1339. https://doi.org/10.1002/2013JD020742.

Seo, K.H., Frierson, D.M., Son, J.H., 2014. A mechanism for future changes in Hadley circulation strength in CMIP5 climate change simulations. Geophys. Res. Lett. 41 (14), 5251–5258. https://doi.org/10.1002/2014GL060868.

Sepulchre, P, Caubel, A, Ladant, J B, et al., 2020. IPSL-CM5A2–an Earth system model designed for multi-millennial climate simulations. Geosci. Model Dev. 13 (7), 3011–3053. https://doi.org/10.1029/2019MS002010.

Sloan, L.C., Crowley, T.J., Pollard, D., 1996. Modeling of middle Pliocene climate with the NCAR GENESIS general circulation model. Mar. Micropaleontol. 27 (1–4), 51–61. https://doi.org/10.1016/0377-8398(95)00063-1.

Smith, R, Jones, P, Briegleb, B, et al., 2010. The parallel ocean program (POP) reference manual ocean component of the community climate system model (CCSM) and community earth system model (CESM). LAUR-01853 141, 1–140.

Sohn, B.J., Lee, S., Chung, E.S., et al., 2016. The role of the dry static stability for the recent change in the Pacific Walker circulation. J. Clim. 29 (8), 2765–2779. https://doi.org/10.1175/JCLI-D-15-0374.1.

Stepanek, C., Samakinwa, E., Knorr, G., Lohmann, G., 2020. Contribution of the coupled atmosphere–ocean–sea ice–vegetation model cosmos to the Pliomip2. Clim. Past 16, 2275–2323. https://doi.org/10.5194/cp-16-2275-2020.

Sun, Y., Ramstein, G., Contoux, C., et al., 2013. A comparative study of large-scale atmospheric circulation in the context of a future scenario (RCP4. 5) and past warmth (mid-Pliocene). Clim. Past 9 (4), 1613–1627. https://doi.org/10.5194/cp-9-1613-2013.

Sun, Y., Zhou, T., Ramstein, G., et al., 2016. Drivers and mechanisms for enhanced summer monsoon precipitation over East Asia during the mid-Pliocene in the IPSL-CM5A. Clim. Dynam. 46 (5–6), 1437–1457. https://doi.org/10.1007/s00382-015-2656-4.

Sun, Y., Ramstein, G., Li, L.Z., et al., 2018. Quantifying East Asian summer monsoon dynamics in the ECP4.5 scenario with reference to the mid-Piacenzian Warm Period. Geophys. Res. Lett. 45 (22) https://doi.org/10.1029/2018GL080061, 12,523-12,533.

Sun, Y., Li, L.Z., Ramstein, G., et al., 2019. Regional meridional cells governing the interannual variability of the Hadley circulation in boreal winter. Clim. Dynam. 52, 831–853. https://doi.org/10.1007/s00382-018-4263-7.

Tan, N., Contoux, C., Ramstein, G., et al., 2020. Modeling a modern-like pCO_2 warm period (Marine Isotope Stage KM5c) with two versions of an Institut Pierre Simon Laplace atmosphere–ocean coupled general circulation model. Clim. Past 16 (1), 1–16. https://doi.org/10.5194/cp-16-1-2020.

Tierney, J.E., Poulsen, C.J., Montañez, I.P., et al., 2020. Past climates inform our future. Science 370 (6517), eaay3701. https://doi.org/10.1126/science.aay3701.

Xia, Y., Hu, Y., Liu, J., 2020. Comparison of trends in the Hadley circulation between CMIP6 and CMIP5. Sci. Bull. 65 (19), 1667–1674. https://doi.org/10.1016/j.scib.2020.06.011.

Zhang, Q., Berntell, E., Axelsson, J., et al., 2021. Simulating the mid-Holocene, last interglacial and mid-Pliocene climate with EC-Earth 3-LR. Geosci. Model Dev. (GMD) 14 (2), 1147–1169. https://doi.org/10.5194/gmd-14-1147-2021.

Zhang, S., Hu, Y., Yang, J., et al., 2023. The Hadley circulation in the Pangea era. Sci. Bull. 68 (10), 1060–1068. https://doi.org/10.1016/j.scib.2023.04.021.

Zhang, H.B., Li, M.T., Peng, W.B., et al., 2022. No major temporal provenance variation on the Chinese Loess Plateau since the late Miocene — insight from stable heavy mineral ratios. Geosyst. Geoenviron. 1 (2), 1000022 https://doi.org/10.1016/j.geogeo.2022.100022.

Zheng, J., Zhang, Q., Li, Q., et al., 2019. Contribution of sea ice albedo and insulation effects to Arctic amplification in the EC-Earth Pliocene simulation. Clim. Past 15 (1), 291–305. https://doi.org/10.5194/cp-15-291-.